nature nanotechnology
SUPPLEMENTARY INFORMATION
DOI: 10.1038/NNANO.2012.147

Probing the Conductance Superposition Law in Single Molecule Circuits with Parallel Paths

H. Vazquez[1], R. Skouta[2], S. Schneebeli[2], M. Kamenetska[1], R.Breslow[2*],
L.Venkataraman[1*], M.S.Hybertsen[3*]

[1]*Department of Applied Physics and Applied Mathematics, Columbia University*
[2]*Department of Chemistry, Columbia University, NY*
[3]*Center for Functional Nanomaterials, Brookhaven National Laboratory*

Email: rb33@columbia.edu; lv2117@columbia.edu; mhyberts@bnl.gov

Contents:

1. **Synthesis Information**
2. **Table of Structures**
3. **Measurement and Data Analysis**
4. **Procedures for Theoretical Calculations**
5. **References**

1. Synthesis Information:

Chemicals: Solvents, inorganic salts, and organic reagents were purchased from commercial sources and used without further purification unless otherwise mentioned.

Chromatography: Merck pre-coated 0.25 mm silica plates containing a 254 nm fluorescence indicator were used ford analytical thin-layer chromatography. Flash chromatography was performed on 230-400 mesh silica (SiliaFlash® P60) from Silicycle.

Spectroscopy: NMR spectra were obtained on a Bruker DPX 300 or 400 MHz spectrometer. Spectra were analyzed with the MestreNova Software (Version 6.1). CI-MS spectra were taken on a Nermag R-10-10 instrument. The 1,4-bis(methylthiomethyl)benzene **(3a)** and the 5, 14-dimethoxy-2- 11-dithia (3. 3) paracyclophane **(5a)** are commercially available from commercial sources (sigma). X-rays were performed in the laboratory of Professor Girard Parkin in the department of chemistry at Columbia University.

Synthesis of various 1,4-bis(methylthiomethyl)benzene derivatives

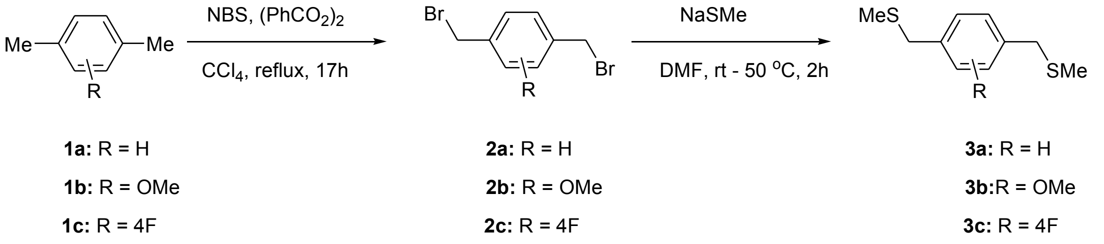

Scheme 1. Synthesis of various 1,4-bis(methylthiomethyl)benzene derivatives.

Preparation of 1,4-bis(methylthiomethyl)benzene derivatives: general protocol (Scheme 1)

Various solutions of **(1a-c)** compounds (1 equiv) were added to a mixture of N-bromosuccinimide (2.1 equiv) and benzoyl chloride (4 mol %) in CCl_4 under argon. The mixtures were refluxed under visible light for 17h then cooled down. The precipitate was filtered out using celite and the solvent was removed under vacuum to provide the 1,4-bis(bromomethyl)benzene derivatives (**2a-c)** as white solid. The latter were heated in dry DMF at 50 °C for 2h in the presence of sodium methanethiolate (2.4 equiv). The mixture was cooled down and water was added. The aqueous layer was extracted with EtOAc three times. The organic layers were dried with Na_2SO_4, filtered and the solvent was evaporated in vacuo. The residue was purified by flash-column chromatography on silica gel to give the desired 1,4-bis(methylthiomethyl)benzene derivatives **(3a-c)**.

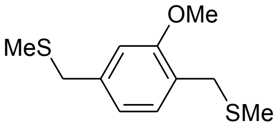

3b

2-methoxy-1,4-bis(methylthiomethyl)benzene (3b, denoted 1OMe in the main text): Following the above general procedure with N-bromosuccinimide (1.37 g, 7.70 mmol), benzoyl chloride (35.5 mg, 0.147 mmol), 2-methoxy-1,4-dimethylbenzene (**1b**) (0.5 g, 3.67 mmol) and sodium methanethiolate (0.61 g, 8.83 mmol), the crude reaction mixture was purified by column chromatography (hexane : EtOAc =20:1) to give the 1,4-bis(methylthiomethyl)benzene **(3b)** (0.54 g, 2.36 mmol, 64% (2 steps)). ^{1}H NMR ($CDCl_3$, 300MHz, ppm) δ 7.14(d, J = 7.8Hz, 1H), 6.85(s, 1H), 6.82(d, J = 7.8Hz, 1H), 3.85(s, 3H), 3.68(s, 2H), 3.65(s, 2H), 2.04(s, 3H), 2.00(s, 3H); ^{13}C NMR ($CDCl_3$, 75MHz, ppm) δ 157.5, 138.6, 130.1, 125.5, 120.9, 111.2, 55.6, 38.5, 32.4, 15.4, 15.1; MS (FAB+, *m/z*) 228; HRMS calcd for $C_{11}H_{16}OS_2$: 228.0905; found: 228.0902.

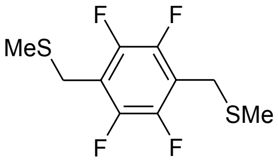

3c

1,2,4,5-tetrafluoro-3,6-bis(methylthiomethyl)benzene (3c, denoted 1F in the main text): Following the above general procedure with N-bromosuccinimide (1.09g, 6.17 mmol), benzoyl chloride (34 mg, 0.14 mmol), 1,2,4,5-tetrafluoro-3,6-dimethylbenzene (**1c**) (0.5 g, 2.81 mmol) and sodium methanethiolate (0.472 g, 6.74 mmol), the crude reaction mixture was purified by column chromatography (hexane: EtOAc= 50:1) to give the 1,4-bis(methylthiomethyl)-benzene **(3c)** (0.44 g, 1.629 mmol, 58% (2 steps)). ^{1}H NMR ($CDCl_3$, 300MHz, ppm) δ 3.75(s, 4H), 2.12(s, 6H); ^{13}C NMR ($CDCl_3$, 75MHz, ppm) δ 146.2, 142.9, 116.9, 25.0, 15.7; ^{19}F NMR δ -140.4 (S, 4F); MS (FAB+, *m/z*) 270; HRMS calcd for $C_{10}H_{10}F_4S_2$: 270.0103; found: 270.0103.

Synthesis of various 2,11-dithia(3.3)paracyclophane derivatives

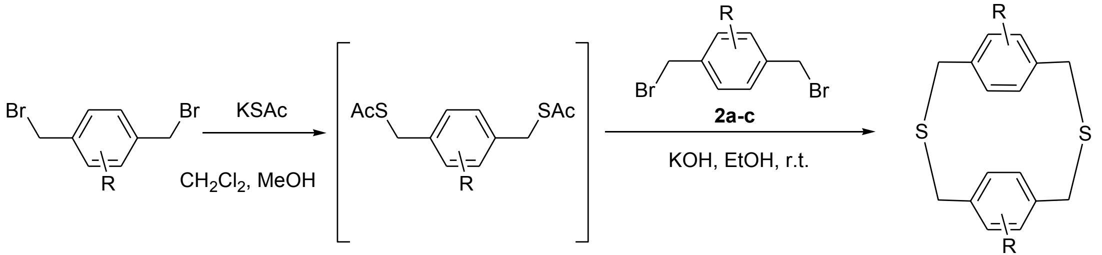

2a: R = H
2b: R = OMe
2c: R = 4F

4a: R = H
4b: R = OMe
4c: R = 4F

5a: R = H
5b:R = OMe
5c: R = 4F

Scheme 2. Synthesis of various 2,11-dithia(3.3)paracyclophane derivatives.

Preparation of various 2,11-dithia(3.3)paracyclophane derivatives: general protocol (Scheme 2)

Potassium thio-acetate (2 equiv) was added to various 1,4-bis(bromomethyl)benzene derivatives (**2a-c)** (1 equiv) in a mixture of CH_2Cl_2: MeOH (1:1 ratio). The mixture was stirred at room temperature for 2h then filtered through a pad of celite. The solvent was removed and the crude 1,4-bis(thio-acetate)benzene derivatives (**4a-c)** were used without further purification in the next step. The crude 1,4-bis(thioacetate)benzene derivatives (**4a-c)** (1 equiv), and the 1,4-bis(bromomethyl) benzene (**2a-c**) (1 equiv) were dissolved in 10 ml of toluene and added, at room temperature, through a syringe pump (0.5 mL / hour) to a solution of Cs_2CO_3 (2.2 equiv) in ethanol (100 mL). The solvent was removed in vacuo. The residue was washed with water and extracted with CH_2Cl_2 three times. The organic layers were dried with Na_2SO_4, filtered and the solvent was evaporated in vacuo. The residue was purified by flash-column chromatography on silica gel (hexane: EtOAc= 50:1) to provide 2,11-dithia(3.3)paracyclophane derivatives (**5a-c)**.

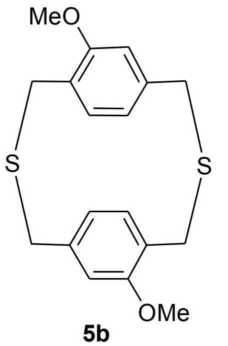

5b

≡

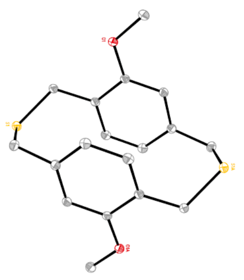

X-ray structure of **5b**

5, 14-dimethoxy-2- 11-dithia (3. 3) paracyclophane (5b, denoted 2OMe in the main text):

Following the above general procedure with 2-methoxy-1,4-bis(thio-acetate)benzene (**4b**) (100 mg, 0.340 mmol), 2-methoxy-1,4-bis(bromomethyl) benzene (**2b**) (96.7 mg, 0.340 mmol) and Cs_2CO_3 (243.7 mg, 0.748 mmol) in ethanol (100 mL), the residue was purified by flash-column chromatography on silica gel (hexane: EtOAc=50:1) to provide the thiocyclophane (**5b)** (58 mg, 0.175 mmol, 51%) which was confirmed by an X-ray structure; ^{1}H NMR ($CDCl_3$, 300MHz, ppm) δ 6.89(d, J = 7.7Hz, 2H), 6.55(s, 2H), 6.46(d, J = 7.7Hz, 2H), 4.33(d, J = 10.8Hz, 2H), 3.87-3.72(m, 10H), 3.34(d, J = 10.8Hz, 2H); ^{13}C NMR ($CDCl_3$, 75MHz, ppm) δ 156.5, 130.5, 120.4, 111.7, 54.9, 38.0, 30.7; MS (FAB+, *m/z*) 332; HRMS calcd for $C_{18}H_{20}O_2S_2$: 332.0905; found: 332.0902.

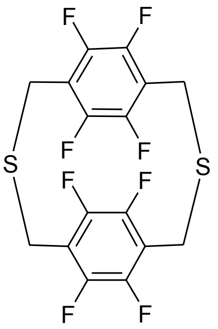

5c

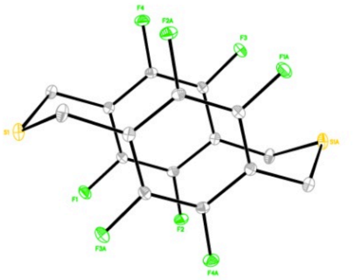

X-ray structure of **5c**

5, 6, 8, 9, 14, 15, 17, 18-octafluoro-2, 11-dithia (3. 3) paracyclophane (5c, denoted 2F in the main text): Following the above general procedure with 2, 3, 5, 6-tetrafluoro-1,4-bis(thioacetate)benzene (**4c**) (122 mg, 0.374 mmol) and 2,3,5,6-tetrafluoro-1,4-bis(bromomethyl)benzene (**2c**) (125.7 mg, 0.374 mmol), the residue was purified by flash-column chromatography on silica gel (hexane: EtOAc= 20:1) to provide the thiocyclophane **(5c)** (111 mg, 0.298 mmol, 80%) which was confirmed by an X-ray structure; ^{1}H NMR ($CDCl_3$, 400MHz, ppm) δ 3.96(s, 8H); ^{13}C NMR ($CDCl_3$, 75MHz, ppm) δ 144.7(d, J_{FC} = 240 Hz), 115.1(m, CF), 24.9; ^{19}F NMR δ -140.4 (S, 8F); MS (EI+, *M+1*) 416; HRMS calcd for $C_{16}H_8F_8S_2$: 415.9940; found: 415.9913. The NMR spectra of the compound (**5c**) are consistent with ones reported in the literature[1].

General scheme for the synthesis of 2,7-bis(methylthiomethyl)-9H-fluorene 3d, denoted 1Fl in the main text (Scheme 3).

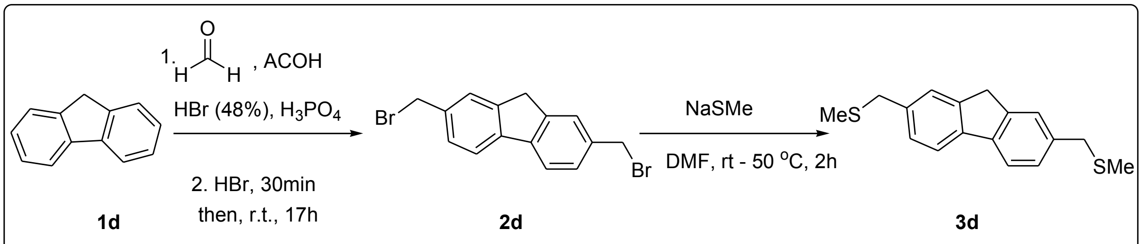

Scheme 3. Synthesis of 2,7-bis(methylthiomethyl)-9*H*-fluorene **3d**.

Synthesis of 2,7-bis(bromomethyl)-9H-fluorene 2d (Scheme 3).

The fluorene (**1d)** (5g, 30.08 mM) was mixed with formaldehyde (3.6g, 120.30 mM), phosphoric acid 96.9 mL) and HBr (48%, 9.4mL) in AcOH (12mL). The mixture was stirred at room temperature for 6 hours then cooled down to 0 ^{o}C before HBr gas was bubbled for 30 minutes. The reaction mixture was stirred at room temperature for 17h. The precipitate was filtered out and heated under reflux in acetone for 1h. The white solid was filtered and recrystallized in acetone to provide the desired 2,7-bis(bromomethyl)-9H-fluorene **2d** (6g, 23.8 mmol, 79%). ^{1}H NMR ($CDCl_3$, 300MHz, ppm) δ 7.72(d, J = 8.1Hz, 2H), 7.57(s, 2H), 7.41(d, J = 8.1Hz, 2H), 4.60 (s, 4H), 3.89(s, 2H); MS (FAB+, *m/z*) 352. The ^{1}H NMR spectra of the compound (**2d**) is consistent with one reported in the literature[2].

Synthesis of 2,7-bis(methylthiomethyl)-9H-fluorene 3d (Scheme 3).

The 2,7-bis(bromomethyl)-9H-fluorene **2d** (400 mg, 1.13 mM) was heated in dry DMF at 50 ^{o}C for 2h in the presence of sodium methanethiolate (191.1 mg, 2.72 mM). The mixture was cooled down and water was added. The aqueous layer was extracted with EtOAc three times. The organic layers were dried with Na_2SO_4, filtered and the solvent was evaporated in vacuo. The residue was purified by flash-column chromatography on silica gel to give the desired 2,7-bis(methylthiomethyl)-9H-fluorene **3d** (241 mg, 0.85 mM, 75%). ^{1}H NMR ($CDCl_3$, 300MHz, ppm) δ 7.69(d, J = 8.1Hz, 2H), 7.48(s, 2H), 7.27(d, J = 8.1Hz, 2H), 3.78 (s, 2H), 3.75 (s, 4H), 2.02 (s, 6H); MS (FAB+, *m/z*) 286.

Synthesis of the 2,14-dithia[3.3](2.7)fluorenophane 5d, denoted 2Fl in the main text (Scheme 4).

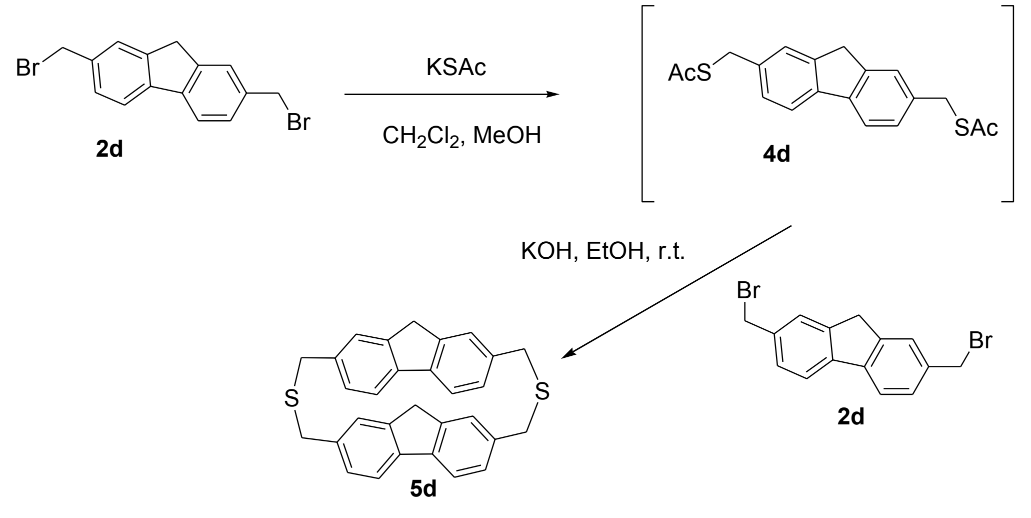

Scheme 4. Synthesis of 2,14-dithia[3.3](2.7)fluorenophane **5d**.

Potassium thio-acetate (64.7mg, 0.568mmol, 2 equiv) was added to the 2,7-bis(bromomethyl)-9H-fluorene (**2d)** (100mg, 0.284 mmol, 1 equiv) in a mixture of CH_2Cl_2: MeOH (1:1 ratio). The mixture was stirred at room temperature for 2h then filtered through a pad of celite. The solvent was removed and the crude 2,7-bis(thio-acetate)-9H-fluorene (**4d)** was used without further purification in the next step. The crude 2,7-bis(thio-acetate)-9H-fluorene (**4d)** (48.5 mg, 0.142 mmol, 1 equiv), and the 2,7-bis(bromomethyl)-9H-fluorene (**2d)** (50 mg, 0.142 mmol, 1 equiv) were dissolved in 10 ml of toluene and added, at room temperature, through a syringe pump (0.5 mL / hour) to a solution of Cs_2CO_3 (2.2 equiv) in ethanol (100 mL). The solvent was removed in vacuo. The residue was washed with water and extracted with CH_2Cl_2 three times. The organic layers were dried with Na_2SO_4, filtered and the solvent was evaporated in vacuo. The residue was purified by flash-column chromatography on silica gel (hexane: EtOAc= 5:1) to provide the desired 2,14-dithia[3.3](2.7)fluorenophane **5d** (41 mg, 0.093 mM, 66%). ^{1}H NMR ($CDCl_3$, 300MHz, ppm) δ 7.65(d, J = 8.1Hz, 4H), 7.46(s, 4H), 7.24(d, J = 8.1Hz, 4H), 3.77 (s, 2H), 3.73 (s, 8H); MS (FAB+, *m/z*) 448. The ^{1}H NMR spectra of the compound **5d** is consistent with one reported in the literature[2].

Synthesis of 2,11-dithia(3.3)paracyclophane 7, denoted 1a in the main text (Scheme 5)

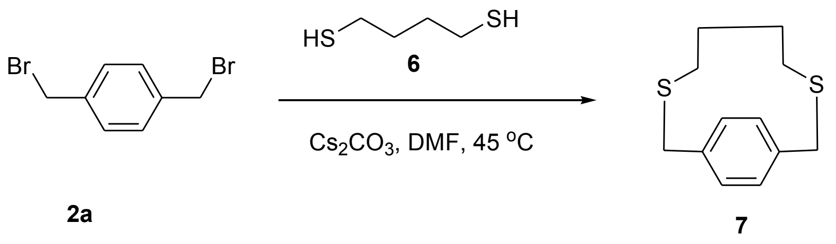

Scheme 5. Synthesis of the 2,11-dithia(3.3)paracyclophane **7**.

The 1,4-bis(bromomethyl) benzene (**2a**) (100mg, 0.381mmol, 1 equiv) and butane-1,4-dithiol (**6**) (0.381mmol, 1 equiv) were dissolved in 10 ml of toluene and added, at 45 ^{o}C, through a syringe pump (0.5 mL / hour) to a solution of Cs_2CO_3 (2.2 equiv) in DMF (50 mL). The mixture was diluted with water and extracted with CH_2Cl_2 three times. The organic layers were dried with Na_2SO_4, filtered and the solvent was evaporated in vacuo. The residue was purified by flash-column chromatography on silica gel (hexane: EtOAc= 50:1) to provide 2,11-dithia(3.3)paracyclophane **(7)** (56mg, 0.251, 66%). ^{1}H NMR ($CDCl_3$, 400MHz, ppm) δ 7.29(s, 4H), 3.77(s, 4H), 2.05(t, J = 7.2Hz, 4H), 0.74(d, J = 7.2Hz, 4H); ^{13}C NMR ($CDCl_3$, 125MHz, ppm) δ 137.9, 130.3, 36.9, 30.59, 28.5; MS (FAB+, *m/z*) 224; HRMS calcd for $C_{18}H_{20}O_2S_2$: 224.0693; found: 224.0687.

2. Table of Structures:

1

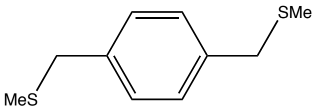

2

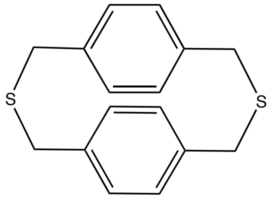

1a

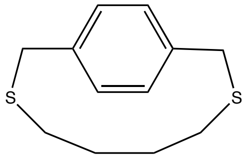

1OMe

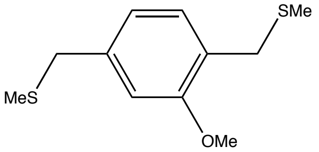

2OMe

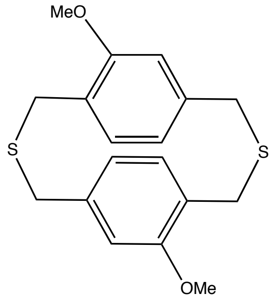

1F

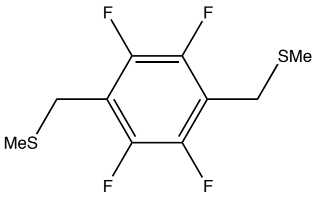

2F

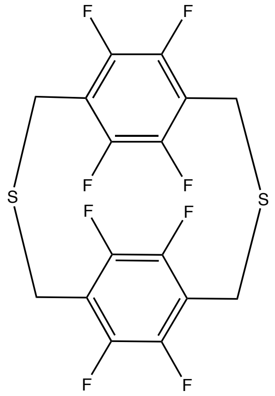

1Fl

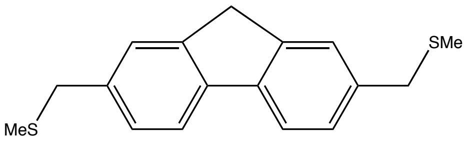

2Fl

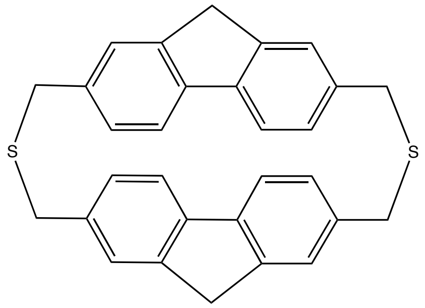

SI Table S1*: Structure of all molecules investigated.*

3. Measurement and Data Analysis:

We measured the molecular conductance of all molecules by repeatedly forming and breaking Au point contacts in 1 mM 1,2,4 trichlorobenzene solution of the molecules with a home-built, simplified STM[3]. A freshly cut gold wire (0.25 mm diameter, 99.999% purity, Alfa Aesar) was used as the tip, and UV/ozone cleaned Au substrate (mica with 100 nm Au, 99.999% purity, Alfa Aesar) was used as the substrate. The STM operates in ambient conditions at room temperature and the junctions were broken in a dilute, 1mM, solution of target molecules in 1,2,4-trichlorobenzene (Sigma-Aldrich, 99% purity). To ensure that each measurement started from a different initial atomic configuration of the electrodes, the electrodes were pulled apart only after being brought into contact with the Au surface, indicated by a conductance greater than a few G_0. Prior to adding a molecular solution between the tip and substrate, 1000 conductance traces were first collected without molecules to ensure that there were no contaminations in the STM set-up. Two-dimensional histograms were constructed from over 10000 measured conductance trace for each compound considered. Conductance traces consists of conductance data acquired every 25 μs, measured as a function of tip-sample displacement at a constant 15 nm/s velocity. Since gold and molecular conductance plateaus occur in random locations along the entire displacement axis (x-axis) within the measured range, we first set the origin of our displacement axis at the point in the conductance traces where the gold-gold contact breaks and the conductance drops below G_0. This well-defined position on the x-axis is determined individually for each trace using an unbiased automated algorithm. For about 5% of the measured traces, this position cannot be determined and these traces are not used for further analysis. Each data point on the digitized conductance trace now has a conductance coordinate (along the y-axis) and a position coordinate (along the x-axis). These data are binned using a linear scale along the displacement axis and a log-scale along the conductance to generate a 2D histogram.

Additional Data:

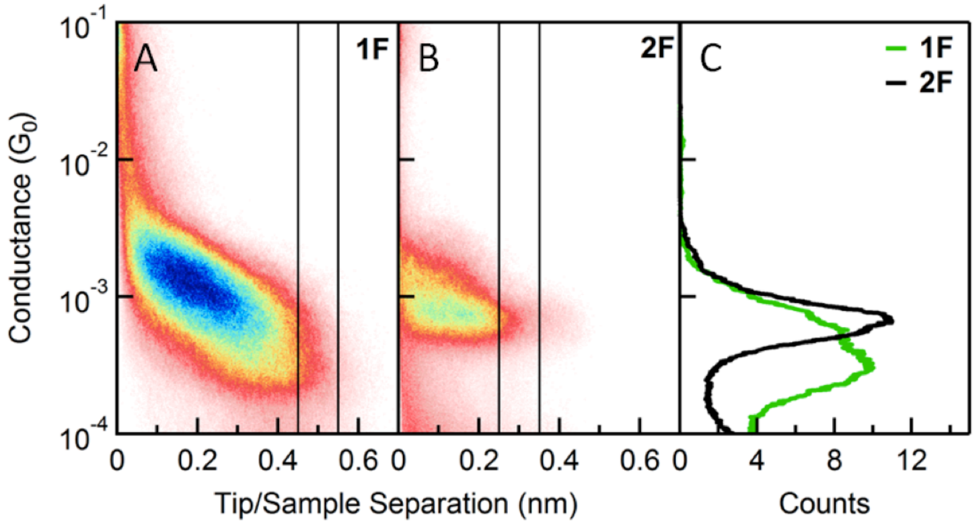

SI Figure S1: *2D conductance histograms for junctions with molecules **1F** (A) and **2F** (B) as a function of tip/substrate separation after breaking the Au-Au contact. C) Conductance profile determined from the 2D histogram for **1F** (green) and **2F** (black) by averaging over the region of width 0.1 nm shown by the vertical lines in (A) and (B).*

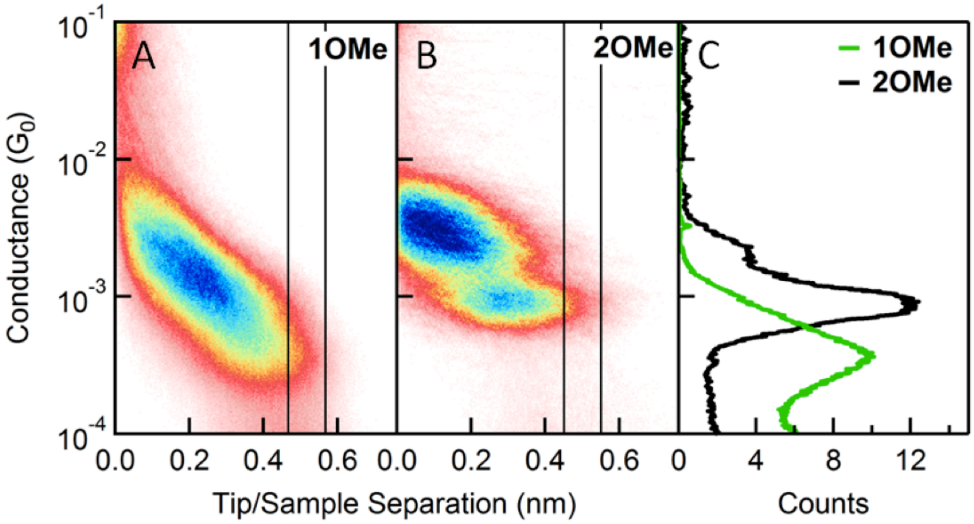

SI Figure S2: *2D conductance histograms for junctions with molecules **1OMe** (A) and **2OMe** (B) as a function of tip/substrate separation after breaking the Au-Au contact. C) Conductance profile determined from the 2D histogram for **1OMe** (green) and **2OMe** (black) by averaging over the region of width 0.1 nm shown by the vertical lines in (A) and (B).*

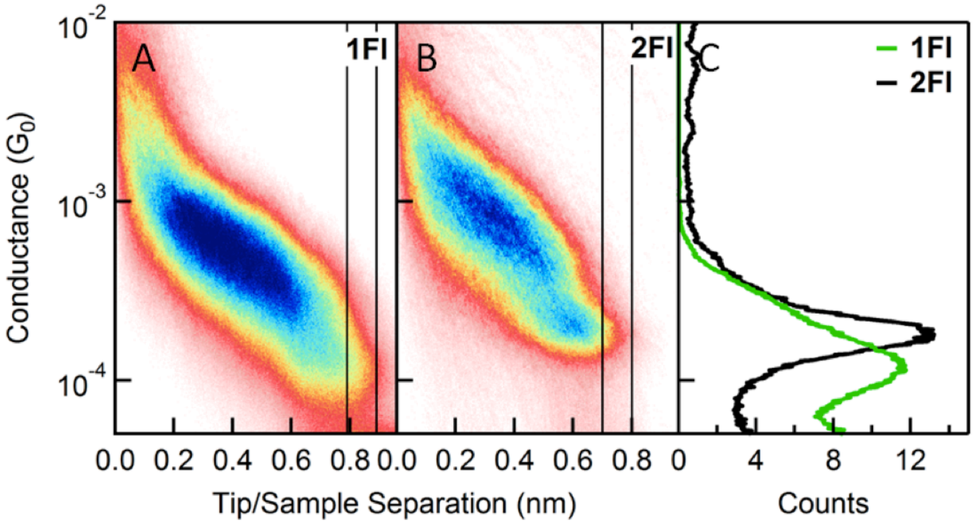

SI Figure S3: *2D conductance histograms for junctions with molecules* ***1Fl*** *(A) and* ***2Fl*** *(B) as a function of tip/substrate separation after breaking the Au-Au contact. C) Conductance profile determined from the 2D histogram for* ***1Fl*** *(green) and* ***2Fl*** *(black) by averaging over the region of width 0.1 nm shown by the vertical lines in (A) and (B).*

4. Procedures for Theoretical Calculations:

Model Approach:

We first qualitatively describe the law of current superposition in single and double backbone molecules using a model Hamiltonian to represent the essential frontier orbitals and a Green's function approach to the junction transmission[4-6]. We describe each molecular backbone with two levels (E_{Hi}, E_{Li}), which correspond to its frontier orbitals, where the subindices H and L refer to HOMO and LUMO, respectively, and i=1, 2 labels the molecular backbone. In the case of **2**, the backbone states interact with each other via a hopping term $-t$ that captures the through space coupling. Each backbone level is connected to gateway states $E_{L,R}$ in the electrode links through a coupling term τ. The model Hamiltonian for the frontier orbitals of **2** is then:

$$H = \begin{pmatrix} E_L & -\tau & -\tau & -\tau & -\tau & 0 \\ -\tau & E_{H1} & -t & 0 & 0 & \tau \\ -\tau & -t & E_{H2} & 0 & 0 & \tau \\ -\tau & 0 & 0 & E_{L1} & -t & -\tau \\ -\tau & 0 & 0 & -t & E_{L2} & -\tau \\ 0 & \tau & \tau & -\tau & -\tau & E_R \end{pmatrix} \tag{1}$$

The relative sign of the coupling terms between each backbone state and the L or R leads captures the different number of nodes in the HOMO and LUMO π states on the backbones. The model Hamiltonian for **1** is similar, but it is represented by a 4×4 matrix. To calculate the transmission properties with this model Hamiltonian, we renormalize the gateway state levels $E_{L,R}$ by a self-energy which represents the interaction with the extended states in each electrode. In the simplest approximation, it can be described by a constant imaginary term ($E_{L,R} \rightarrow E_{L,R} - i\,\Gamma/2$). The retarded Green's function for the model junction is then:

$$G = (E - H)^{-1} =$$

$$= \begin{pmatrix} E - E_L + \mathrm{i}\frac{\Gamma}{2} & \tau & \tau & \tau & \tau & 0 \\ \tau & E - E_{H1} & t & 0 & 0 & -\tau \\ \tau & t & E - E_{H2} & 0 & 0 & -\tau \\ \tau & 0 & 0 & E - E_{L1} & t & \tau \\ \tau & 0 & 0 & t & E - E_{L2} & \tau \\ 0 & -\tau & -\tau & \tau & \tau & E - E_R + \mathrm{i}\frac{\Gamma}{2} \end{pmatrix}^{-1} \tag{2}$$

Finally, the transmission is given by $T(E) = \Gamma^2 |G_{LR}(E)|^2$, where the indices on G refer to the component of the matrix that couples to the left and right electrode respectively; physically this represents the effective propagation from the left gateway state to the right gateway state.

The transmission spectra in Fig. 1D for single- and double-backbone molecules were generated by numerically solving equation (2) using the following parameters: $E_{L,R} = -1eV$, $E_{H,} = -2.4eV$, $E_{Li} = +2.0eV$, $t = 0.3eV$, $\tau = 0.3eV$, $\Gamma = +2eV$. For the double backbone case, a slight asymmetry in the backbone states was introduced, $E_{H1,L1} \rightarrow E_{H1,L1} - \delta$, $E_{H2,L2} \rightarrow E_{H2,L2} + \delta$, with $\delta = 0.1eV$. This small asymmetry gives rise to some parasitic transmission through the antibonding backbone resonance, as described below.

Focusing on a pair of states in backbones **1** and **2**, they can form bonding/antibonding combinations $|B, AB\rangle = \frac{1}{\sqrt{2}}(|1\rangle \pm 2\rangle)$, which diagonalize the molecular 'box' of the Hamiltonian

$$\begin{pmatrix} E_1 & -t \\ -t & E_2 \end{pmatrix} \rightarrow \begin{pmatrix} E_B & 0 \\ 0 & E_{AB} \end{pmatrix} \qquad (3)$$

These bonding/antibonding states are coupled to the gateway nodes via $\tau_{\pm} = \langle L|B, AB\rangle = \langle L \mid \frac{1}{\sqrt{2}}(|1\rangle \pm 2\rangle) = \frac{1}{\sqrt{2}}(\tau_1 \pm \tau_2)$, and similarly for the *R* lead. This expression allows for the coupling τ to be different for the two backbone states (the LUMOs for example). When the states in backbones **1** and **2** are degenerate and equivalent, the bonding (antibonding) wavefunctions are perfectly symmetric (antisymmetric), and the coupling to the leads is exactly $\sqrt{2}\,\tau$ and 0, as shown in Fig 1C. A small difference between the backbone state energies, or in the coupling of each backbone state to the gateway states gives rise to non-zero coupling through the antibonding channels. In the example shown in Fig 1D, this leads to the sharp spikes in the transmission at the energies of the antibonding levels.

If a single frontier orbital dominates (i.e. it is clearly closest to the Fermi energy), then one only needs to consider a single state E_0 per backbone, say the LUMO. At the Fermi level, the corresponding Green's function for the single backbone case reduces to:

$$G_{LR}(E_F) = \frac{\tau^2}{\mathrm{E}_0\left(\frac{\Gamma}{2}\right)^2 - i\Gamma\tau^2} \qquad (4)$$

and the conductance is

$$T(E_F) = \frac{1}{1 + \left(\frac{\mathrm{E}_0\Gamma}{4\tau^2}\right)^2} \qquad (5)$$

Transmission at the Fermi level for a double-backbone system with perfect symmetry between the backbone levels can be calculated from equation (5) by realizing that in this case, only the bonding state will contribute. Substituting the bonding level energy and coupling $\mathrm{E}_b = \mathrm{E}_0 - |t|$ and $\tau_{\mathrm{eff}} = \sqrt{2}\,\tau$ for E_0 and τ, respectively, equation (5) gives

$$T(E_F) = \frac{1}{1 + \left(\frac{\mathrm{E}_b\Gamma}{4\tau_{\mathrm{eff}}^2}\right)^2} \qquad (6)$$

The ratio between the double- and the single- backbone systems is then:

$$\text{ratio }(E_F) = \frac{1 + \left(\frac{\mathrm{E}_0\Gamma}{4\tau^2}\right)^2}{1 + \left(\frac{\mathrm{E}_b\Gamma}{4\tau_{\mathrm{eff}}^2}\right)^2} = \frac{1 + \left(\frac{\mathrm{E}_0\Gamma}{4\tau^2}\right)^2}{1 + \left(\frac{(\mathrm{E}_0 - |t|)\Gamma}{8\tau^2}\right)^2} \qquad (7)$$

In the limit when E_0 and Γ are large compared to 2τ and t, this ratio approaches 4, the ideal result. The model that includes both HOMO and LUMO, Eq. (1), also approaches 4 under the conditions described in the text. Both models give the same result as found by a different argument previously [7].

Transmission calculations:

Structural relaxation calculations of the molecular junctions are carried out using SIESTA[8] with initial structures containing the molecule and Au tips in a 4x4 Au(111) unit cell. The GGA (PBE) approximation is used for exchange-correlation[9]. Au atomic orbitals are described using single-zeta polarized orbitals (with high cutoff radii for tip and surface atoms) and molecular atoms are described by double-zeta polarized orbitals. Initially, the vertical distance is optimized by varying the electrode-electrode separation. The structure containing 6 Au layers is then optimized until the forces on all molecule and tip atoms are smaller than 0.02 eV/Å. We find a binding energy of ~0.9 eV per bond, in agreement with previous work[10]. The C-C interbackbone distance is 3.5 Å.

Subsequent transmission calculations are carried out using TranSIESTA[11] for relaxed geometries built from these optimized structures by adding 3 extra Au layers on each side of the supercell. The transport unit cell contains a total of Au 12 layers (Figure S4).

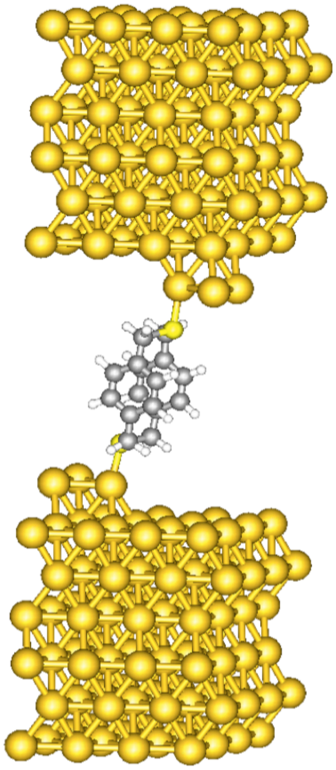

***SI Figure S4**: Unit cell containing molecule **2** used in the transport calculations. White atoms: H, grey: C, yellow: S, golden: Au.*

The electronic structure is calculated using a 5x5 Monkhorst-Pack grid and a 250 Ry real-space cutoff. Transmission spectra are calculated with a 15x15 sampling of the transverse Brillouin zone. The scattering states, the real part of which are presented in the isosurface plots, are generated at the center of the Brillouin zone using the method of Paulsson and Brandbyge[12]. The effect of the electrode tip structure was investigated by checking these results against optimized structures where each tip consists of a single Au adatom. The conductance at the Fermi level differed by ~30% across the different molecules, within the width of the experimental histograms (see Table SI1).

Figures S5A-C show the structure of the molecular junction of **1**, **2** and **1c** structures. The 'cut molecule' **1c** is obtained from the relaxed structure of **2** by removing one backbone and saturating with H atoms. A comparison between the calculated transmission spectra of **1** and **1c** is shown in Figure S5D. Notice that both spectra exhibit the same qualitative features, as molecules **1** and **1c** have the same number of atoms and structure, and differ only in their geometric arrangement at the junction.

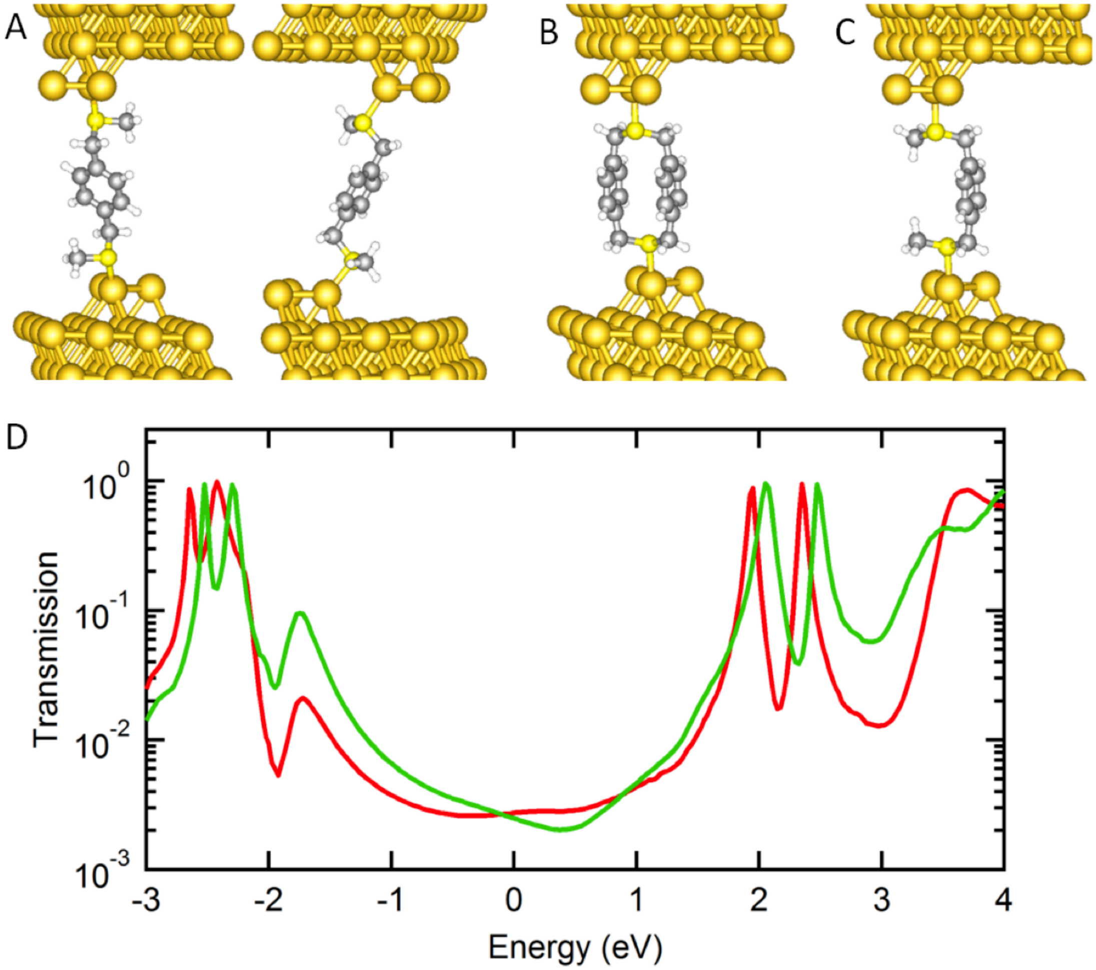

***SI Figure S5**: Optimized junction geometries for the molecular structures of A) **1**; B) **2** and; C) **1c**. White atoms: H, grey: C, yellow: S, golden: Au. D) Calculated transmission spectra of **1** (red) and **1c** (green). The spectra of both single backbone molecules exhibit the same qualitative features.*

Figure S6 shows the junction structure and transmission spectrum of the molecule (**1a**) having a Benzene and a Butane backbone in parallel. Notice that, despite being a double backbone molecule, its electronic properties are those of a single backbone molecule, as it has only one conjugated backbone.

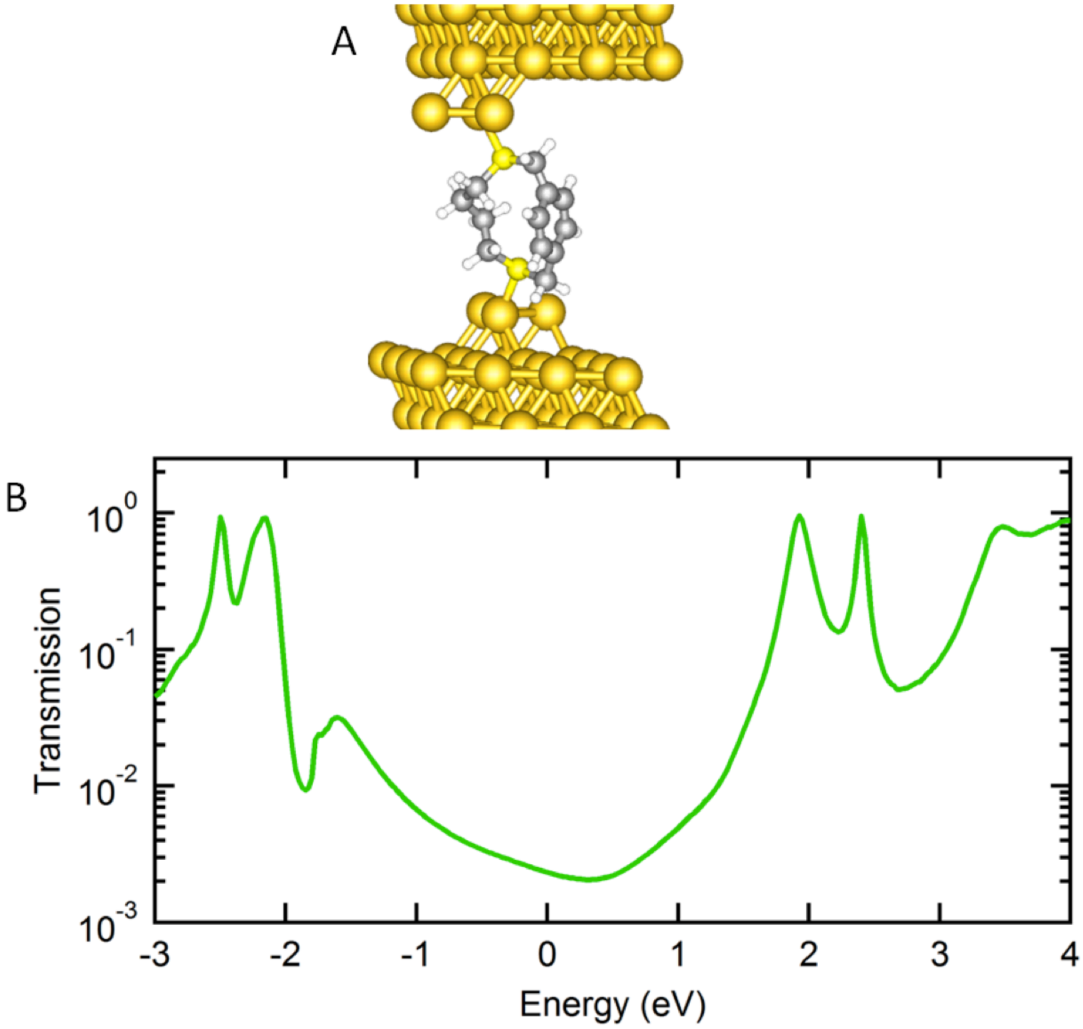

SI Figure S6: *Optimized junction geometries for the molecular structures of A)* ***1a****. White atoms: H, grey: C, yellow: S, golden: Au. B) Calculated transmission spectra of* ***1a****. Notice the similarity in the junction structure and transmission spectrum with the single backbone molecules* ***1c*** *and* ***1*** *(Figure S5).*

The paper shows how the conductance superposition law in single molecule junctions results from the formation of bonding / antibonding pairs between states from each backbone. The main text illustrates this by focusing (Figure 3) on the orbitals that have the largest influence on conductance. These are the state at 2.1 eV of **1c**, and the resulting bonding (1.9 eV) and antibonding (2.5 eV) states of **2**. Figure S7 extends this analysis to the resonances at -2.3 eV and 2.5 eV of **1**, and the corresponding bonding / antibonding pairs of **2**.

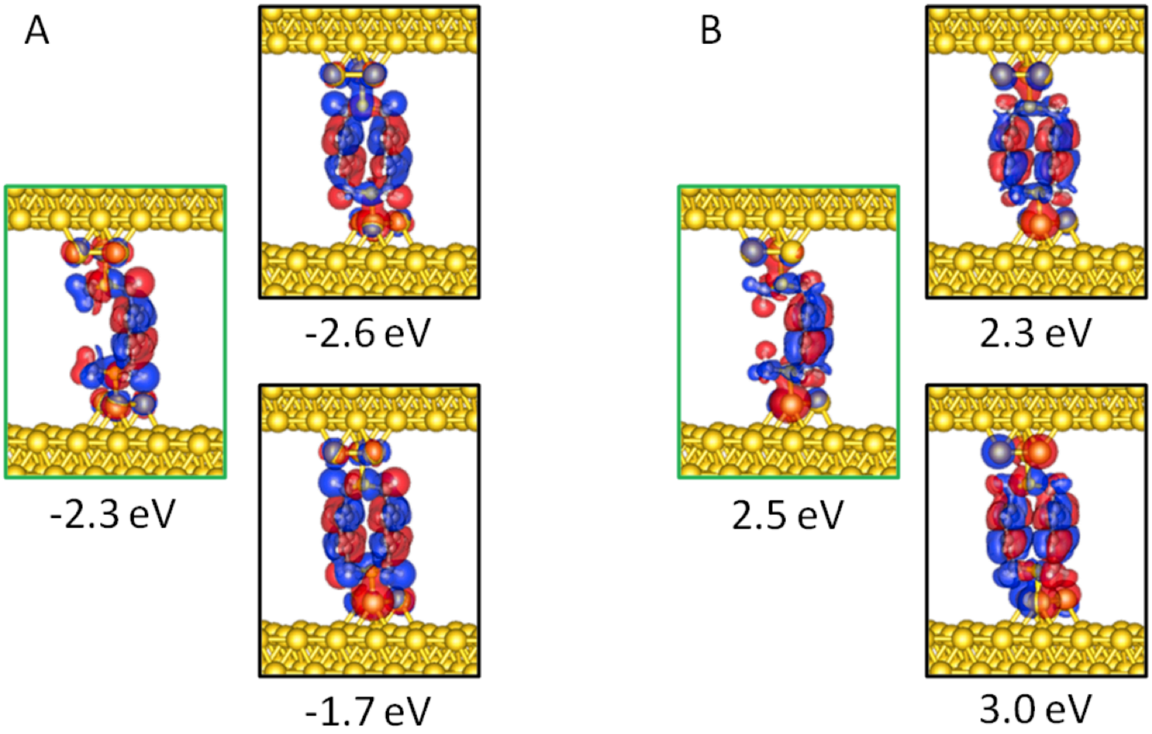

SI Figure S7: *Occupied (A) and unoccupied (B) scattering states of 1 (green), as well as the corresponding bonding/antibonding states of 2 (black).*

Figure S8 shows the molecular junction structure for the case of F and OMe substituents and the corresponding transmission spectra. The same is shown in Figure S9 for molecules having Fluorene backbones.

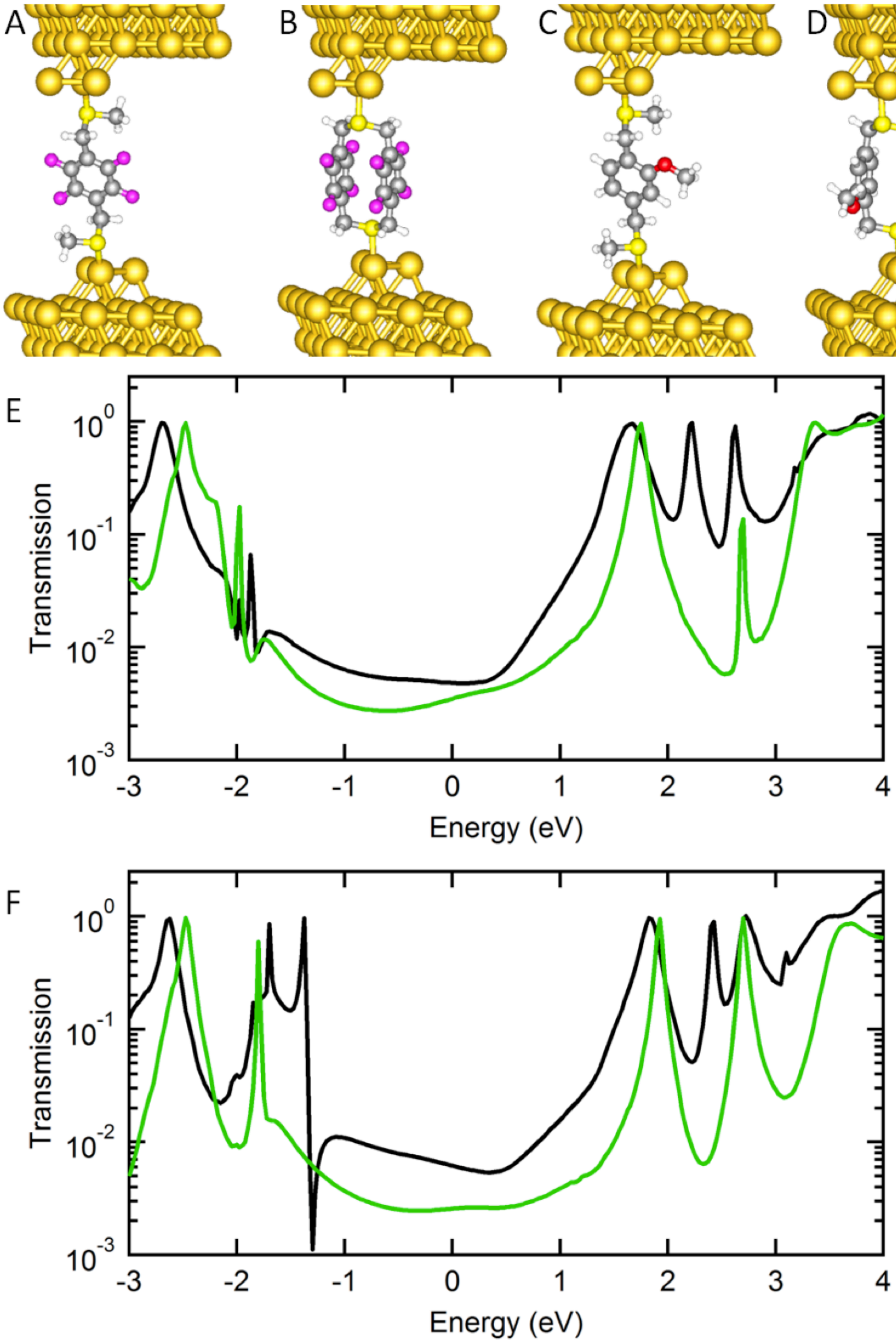

***SI Figure S8**: Optimized junction geometries for the molecular structures of A) **1F**; B) **2F**; C) **1OMe**; D) **2OMe**. White atoms: H, grey: C, yellow: S, pink: F, red: O, golden: Au. Calculated transmission spectra of E) **1F** (green) and **2F** (black) and F) **1OMe** (green) and **2OMe** (black). In both cases, the spectrum of the double backbone molecule shows twice as many transmission peaks as that of the single backbone species.*

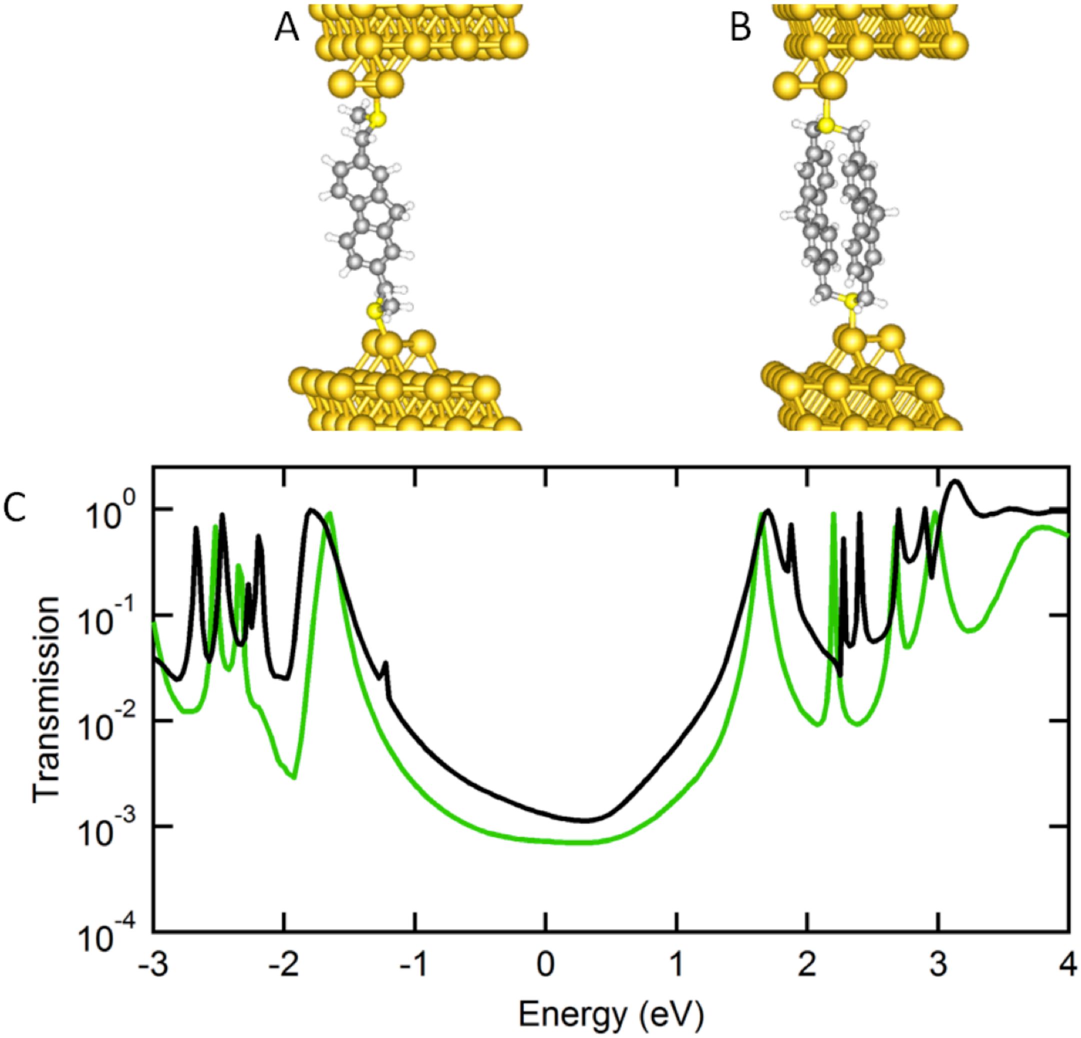

***SI Figure S9**: Optimized junction geometries for the molecular structures of A) **1Fl**; B) **2Fl**. White atoms: H, grey: C, yellow: S, golden: Au. C) Calculated transmission spectra of **1Fl** (green) and **2Fl** (black).*

Number of backbones	**Backbone Structure**	**Calculated conductance G(E_F)**			
		Trimer tips		**Adatom tips**	
1		2.7×10^{-3} G_0	3.0	4.3×10^{-3} G_0	2.0
2		8.2×10^{-3} G_0		8.6×10^{-3} G_0	
1F	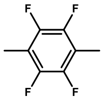	3.5×10^{-3} G_0	1.4	6.4×10^{-3} G_0	0.9
2F		4.8×10^{-3} G_0		5.8×10^{-3} G_0	
1OMe	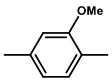	2.6×10^{-3} G_0	2.4	3.8×10^{-3} G_0	1.4
2OMe		6.2×10^{-3} G_0		5.3×10^{-3} G_0	
1Fl	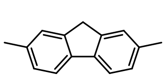	7.2×10^{-4} G_0	1.8	1.1×10^{-3} G_0	1.2
2Fl		1.3×10^{-3} G_0		1.3×10^{-3} G_0	
1a	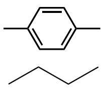	2.3×10^{-3} G_0	—	2.3×10^{-3} G_0	—
1c	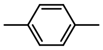	2.5×10^{-3} G_0	—	2.6×10^{-3} G_0	—

***SI Table S2**: Calculated conductance (G_0) at E_F of the different single and double backbone molecules with trimer and adatom tips.*

We correct the DFT-based calculated conductance values of **1c**, **1** and **2** by considering the alignment errors in the position of the relevant frontier orbitals. We have seen (Figure 3) that these are the occupied and empty molecular resonances closest to the Fermi level: the resonance at -1.7 eV and the LUMO-derived peak. For each molecule, we rigidly shift the position of these resonances by an amount which includes self-energy corrections to the molecular level positions and screening effects at the interface. The magnitude of the self-energy shift is calculated from differences in the total energy[13] of the neutral and charged molecule, ensuring that the excitation corresponds to the appropriate molecular orbital (ie. localized on the S atom and on the LUMO, respectively). The screening of these molecular excitations at the junction is described[14] by a classical image charge potential, assuming the charge to be localized on the S atom and at the center of the benzene ring, respectively, and taking the image plane 1Å above the Au(111) atomic plane[15]. We find the occupied resonance at -1.7 eV to be shifted only slightly, while the position of the LUMO-derived peak has to be shifted up by ~0.7-0.8 eV. Specifically, the net shift, which includes both self-energy and image charge contributions, for **1c**, **1** and **2** is -0.2, 0.0 and -0.1 eV for the occupied resonance, and 0.8, 0.7 and 0.7 eV for the unoccupied one, respectively. By fitting the calculated transmission spectra between these resonances to the sum of two lorentzians, we obtain the change in the conductance ratio due to a shift in the resonance position. We find that, within this two lorentzian approximation, the ratio G(**2**)/G(**1c**) is reduced by 7%, while G(**2**)/G(**1**) is reduced by 20%, indicating that the conductance ratio is relatively insensitive to the corrections to the DFT level alignment.

We calculate the conductance of single and double backbone molecules for junctions stretched from their equilibrium electrode-electrode separations. The molecular junctions were stretched from their equilibrium geometries by increasing the electrode-electrode separation and relaxing all tip and molecular atoms. For **1** and **2**, this was done in steps of 0.3Å (SI Figure S10). We find that the conductance ratio G(**2**)/G(**1**) increases as the junction is pulled since the molecular π system of **1** is better coupled to the electrodes, making G(**1**) decrease more rapidly than G(**2**) as the electrode-electrode distance increases. Similar calculations for F and OMe substituents and Fluorene backbones when the junction was stretched by 1.2Å increase in the conductance ratios to 1.5, 2.6 and 2.8, respectively.

However, these substitutions introduce (antibonding) resonances in the double backbone molecules in the energy window of the Au-S gateway states, reducing transmission for energies near the Au-S end resonance (≈-1.7 eV). Since low-bias conductance is affected both by the bonding LUMO-derived peak as well as by this Au-S end resonance, these additional peaks associated with substituents reduce the transmission of the double backbone molecules with respect to **2** in the region below the Fermi level. This makes the ratios G(2)/G(1) for substituents smaller than for the pair **1**-**2**, as measured experimentally.

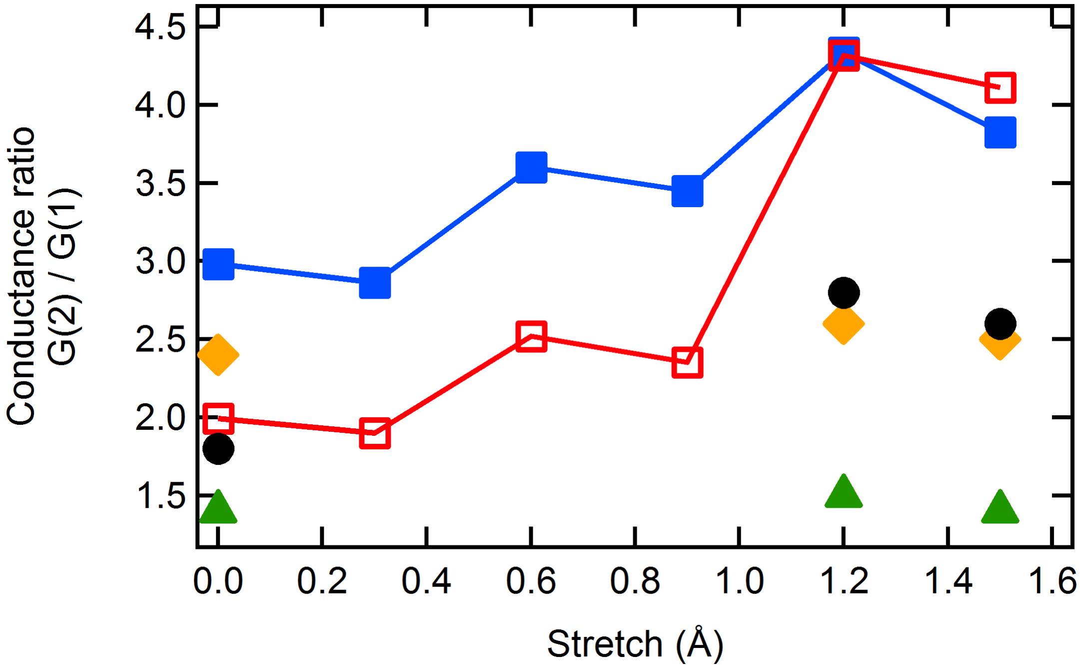

SI Figure S10. *Ratio G(2)/G(1) between the calculated conductance at* E_F *of double backbone molecules and the corresponding single backbone analog, as a function of vertical stretching from their respective electrode-electrode equilibrium separations, for different molecular junctions.* ***1-2*** *backbones with trimer (adatom) tips: blue filled (open squares.* ***1F-2F*** *backbones with trimer tips: green triangles.* ***1OMe-2OMe*** *backbones with trimer tips: orange diamonds.* ***1Fl-2Fl*** *backbones with trimer tips: black circles.*

References:

1 Filler, R., Cantrell, G.L., Wolanin, D., & Naqvi, S.M., Synthesis of polyfluoroaryl[2.2]cyclophanes. *J. Fluorine Chem.* 30, 399-414 (1986).

2 Haenel, M.W., Irngartinger, H., & Krieger, C., Transannular Interaction in [M.N]Phanes .27. Models for Excimers and Exciplexes - [2.2]Phanes of Fluorene, 9-Fluorenone, and 9-Fluorenyl Anion. *Chem. Ber.* 118 (1), 144-162 (1985).

3 Venkataraman, L. *et al.*, Single-Molecule Circuits with Well-Defined Molecular Conductance. *Nano Lett.* 6 (3), 458 - 462 (2006).

4 Nitzan, A., Electron transmission through molecules and molecular interfaces. *Annual Review of Physical Chemistry* 52, 681-750 (2001).

5 Datta, S., *Quantum Transport - Atom to Transistor*. (Cambridge University Press, 2005).

6 Hybertsen, M.S. *et al.*, Amine-linked single-molecule circuits: systematic trends across molecular families. *J. Phys.:Cond. Mat.* 20 (37), 374115 (2008).

7 Magoga, M. & Joachim, C., Conductance of molecular wires connected or bonded in parallel. *Phys. Rev. B* 59 (24), 16011 (1999).

8 Soler, J.M. *et al.*, The SIESTA method for ab initio order-N materials simulation. *J. Phys.:Cond. Mat.* 14 (11), 2745-2779 (2002).
9 Perdew, J.P., Burke, K., & Ernzerhof, M., Generalized gradient approximation made simple. *Phys. Rev. Lett.* 77 (18), 3865-3868 (1996).
10 Park, Y.S. *et al.*, Frustrated Rotations in Single-Molecule Junctions. *J. Am. Chem. Soc.* 131 (31), 10820-10821 (2009).
11 Brandbyge, M., Mozos, J.L., Ordejon, P., Taylor, J., & Stokbro, K., Density-functional method for nonequilibrium electron transport. *Phys. Rev. B* 65 (16), 165401 (2002).
12 Paulsson, M. & Brandbyge, M., Transmission eigenchannels from nonequilibrium Green's functions. *Phys. Rev. B* 76 (11), 115117 (2007).
13 Jaguar, Jaguar v7.8 (Schrodinger, L.L.C., New York, NY 2011).
14 Quek, S.Y. *et al.*, Amine-gold linked single-molecule circuits: Experiment and theory. *Nano Lett.* 7 (11), 3477-3482 (2007).
15 Smith, N.V., Chen, C.T., & Weinert, M., Distance of the Image Plane from Metal-Surfaces. *Phys. Rev. B* 40 (11), 7565-7573 (1989).